

Optical Absorption and Zero Field Splitting Modeling: Mn^{2+} Introduced $\text{Mg Rb}_2 (\text{SO}_4)_2 \cdot 6\text{H}_2\text{O}$ Single Crystals

Maroj Bharati ¹, Vikram Singh ¹, Ram Kripal ² 

¹Department of Physics, Nehru Gram Bharti (DU), Jamunipur, Prayagraj, India

²EPR Laboratory, Department of Physics, University of Allahabad, Prayagraj-211002, India

Received 08 January 2026

Abstract. The splitting parameters of the crystal field and zero field of Mn^{2+} introduced $\text{Mg Rb}_2 (\text{SO}_4)_2 \cdot 6\text{H}_2\text{O}$ (MRS) single crystals have been modeled with superposition model. The zero field splitting parameters found are in fair match with those obtained experimentally from EPR. Mn^{2+} : MRS crystals optical spectra are calculated employing crystal field analysis (CFA) program. A fair agreement is obtained here also with the experimental energy levels.

KEY WORDS: Inorganic compounds, Single crystal, Crystal fields, Zero field splitting, Superposition model, Electron paramagnetic resonance.

1 Introduction

Studies using Electron Paramagnetic Resonance (EPR) spectroscopy on transition metal ions reveal details such as site symmetry and free electron delocalization. Mn^{2+} systems typically have complex EPR spectra because of their “fine structure” and “hyperfine structure”. Whereas hyperfine structure results from the interaction of the electron spin with the nuclear spin, fine structure is caused by the interaction of the electron spins within themselves. The Mn^{2+} ion is a very intriguing probe to thoroughly examine site symmetries because its zero-field splitting (fine structure) parameter is extremely sensitive to even slight distortions from higher symmetry. EPR study of Mn^{2+} , a high spin d^5 ion, has been done quite extensively in octahedral, tetrahedral and cubic environments [1–7].

The superposition model (SPM) has been an important tool for probing the local structure of the singlet ground state ion in different crystals [8, 9]. The SPM is useful in modeling the crystal field (CF) and zero field splitting (ZFS) parameters for many other applications [10–14]. SPM and the point-charge model [15–17]

are often used to find the crystal field (CF) parameters. SPM has been proposed for CF under certain assumptions [18]: (1) The CF at a paramagnetic ion can be expressed as an algebraic sum of the contributions of the other ions in the crystal; (2) All major CF contributions from each ion in the crystal are axially symmetric with respect to their position vector when the paramagnetic ion is located at the origin of a selected coordinate system; (3) Only nearby or coordinated ions (ligands) must have their CF contributions taken into account; (4) A single ligand's CF contribution can be transferred to other host crystals. Using the host crystal's X-ray structural information, each ligand's steady spherical polar coordinate (R_L, θ_L, Φ_L) is important for analysis of SPM on the CF. Ionic bonding, ionic size, and ionic charge mismatches are likely to cause some local distortion when transition metal ions are incorporated. Experimental spin-Hamiltonian parameters for Mn^{2+} and Fe^{3+} in CaO and MgO crystals have been critically analyzed [19] providing the SPM parameters and showing that the CF for 3d ions satisfies the superposition principle. SPM intrinsic parameters based on reliable ligand distances have been estimated for the alkali earth oxides [20]. The crystals of general formula $\text{A}_2^+\text{B}^{2+}(\text{XO}_4)_2 \cdot 6\text{H}_2\text{O}$ are known as Tutton salt single crystals with A being a monovalent cation, B being a divalent cation (usually a transition metal ion) and X being sulfur or selenium [21, 22]. Tutton salt crystals are well known isostructural crystal family with the same monoclinic symmetry, the space group $\text{P}2_1/a$ and two formula units per unit cell $Z = 2$ [23]. Tutton salt crystals are very important crystals as they are largely used in UV filters [24].

Magnesium rubidium sulfate hexahydrate (MRS) crystals belong to the Tutton salt crystal family and crystallize in the monoclinic crystal system. With suitable crystal sizes, high purity and small transparency in the UV region, they are the potential candidates for optoelectronic devices [25]. Beer is made using magnesium sulfate as a brewing salt. It makes the soil richer in sulfur and magnesium. It has numerous medical applications, including in bathing salts, muscle relaxants, and cosmetics. It aids in pregnancy-related issues. It may aid in preventing preeclamptic seizures. It acts as coagulant in making of tofu [26].

Rubidium sulfate is used in making other rubidium salts as the raw materials, for water treatment, or for hematology stain. It is also used on a ceramic bead, as thermoionic detector and as a cathartic [27]. MRS is likely related to the individual uses of its constituent compounds.

EPR study of Mn^{2+} doped MRS has been done at 298 K and the spin-Hamiltonian parameters have been estimated [28]. Magnetic $[\text{Mn}(\text{H}_2\text{O})_6]^{2+}$ complexes are created when the Mn^{2+} ion occupies the divalent sites of the Tutton salt lattice, according to angular variation studies. The orientations are discussed using the $a * bc$ axis system, in which $a*$ is perpendicular to b and c .

In this study, the ZFS parameters D and E are computed for the Mn^{2+} ion in MRS at 298 K (room temperature, RT) using CF parameters from SPM and

perturbation equations [29]. Obtaining the location of the Mn^{2+} ion and the distortion occurring in the MRS crystal is the goal. The parameters of Mn^{2+} ion at the substitutional Zn^{2+} site in the MRS crystal with local distortion show good match with the EPR experimental values. The parameters of CF and the crystal field analysis (CFA) program are employed to calculate the CF energy levels of single crystals of Mn^{2+} introduced MRS. The computed CF energy levels correspond reasonably well with the experimental ones. The study's further aim is to know how well the SPM technique and CF theory apply to Mn^{2+} ions in MRS crystals to generate a database of SPM parameters. This will enable the design of molecular nanomagnets (MNM) and computer simulation of their spectroscopic and magnetic properties. The transition ion-based MNM are single-molecule magnets (SMM) [30], single-chain magnets (SCM) [31], and single ion magnets (SIM) [32]. Due to valuable properties of MNM, like magnetization's macroscopic quantum tunneling and possible applications in high-density information storage and quantum computing, the above systems have attracted a number of scientists and researchers [29, 30]. There are various synthesized SCM or SMM systems with Mn^{2+} and Cr^{3+} ions [33]. Due to the fact that model calculations for simpler crystal systems can serve as a foundation for more complex ones, the parameters of the model in this study may be used for ZFS parameter calculations for Mn^{2+} ions at appropriate sites in molecular nanomagnets. The current modeling technique may be applied in different other ion-host systems to get various crystals of scientific and industrial importance.

2 Crystal Structure

The crystal structure of MRS Tutton salt is monoclinic with space group $P2_1/a$ [34]. The unit cell's parameters are: $Z = 2$, $\beta = 105.98^\circ$, $a = 9.226$, $b = 12.472$ and $c = 6.217$ Å. All other divalent cations in the unit cell are

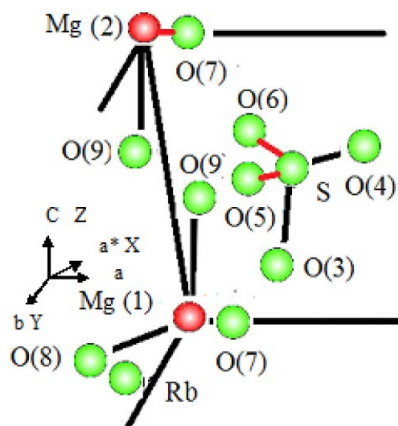


Figure 1. The symmetry-adapted axis system (SAAS) together with room-temperature MRS crystal structure.

in general positions, with the two inequivalent ones positioned at (0, 0, 0) and (1/2, 1/2, 0) points. Water molecules form a slightly warped octahedron around each divalent cation. The symmetry adapted axis system (SAAS) together with room-temperature MRS crystal structure is presented in Figure 1.

3 Crystal Field and Zero Field Splitting Parameter Calculations

The EPR spectra of Mn^{2+} : MRS are analyzed using the spin Hamiltonian [11]:

$$E(S_x^2 - S_y^2) + D\left\{S_z^2 - \frac{1}{3}S(S+1)\right\} + \mu_B B g S = \mathcal{H}, \quad (1)$$

where B , μ_B , g , D and E are the applied magnetic field, Bohr magneton, splitting factor, second rank axial, and second rank rhombic ZFS parameters [35, 36]. The laboratory axes x , y , z and the modified crystallographic axes a^* , b , c (a^* is normal to axes b and c) are displayed in Figure 1. The directions of metal-ligand bonds being mutually perpendicular are referred to as the symmetry adapted axes (SAA) or the local symmetry axes of the site. As shown in Figure 1, the axis- Z of SAAS is along the crystal axis- c , and (X, Y) are perpendicular to the axis- Z . When Mn^{2+} ions are introduced in MRS crystal, they take the position of Mg^{2+} (1) sites with some local distortion in the lattice [37].

The Mn^{2+} ion spin Hamiltonian is taken as [38]

$$\mathcal{H}_o + \mathcal{H}_{so} + \mathcal{H}_{ss} + \mathcal{H}_c = \mathcal{H}, \quad (2)$$

$$\mathcal{H}_c = \sum B_{kq} C_q^{(k)}, \quad (3)$$

where B_{kq} , in Wybourne notation, represent the CF parameters and $C_q^{(k)}$, the spherical tensor operators. $B_{kq} \neq 0$ in the orthorhombic symmetry crystal field only for $k = 2, 4$; $q = 0, 2, 4$. The CF parameters, B_{kq} in MRS are calculated using SPM [38].

The symmetry of the local field about Mn^{2+} ions in MRS crystal is orthorhombic (OR-type I) [11], in which the ZFS parameters D and E are written as follows [39]:

$$D = \left(\frac{3\zeta^2}{70P^2D'}\right)[-B_{20}^2 - 21\zeta B_{20} + 2B_{22}^2], \\ + \left(\frac{\zeta^2}{63P^2G}\right)[-5B_{40}^2 - 4B_{42}^2 + 14B_{44}^2] \quad (4)$$

$$E = \left(\frac{\sqrt{6}\zeta^2}{70P^2D'}\right)[2B_{20} - 21\zeta]B_{22} \\ + \left(\frac{\zeta^2}{63P^2G}\right)[3\sqrt{10}B_{40} + 2\sqrt{7}B_{44}]B_{42}. \quad (5)$$

Here B and C present Racah parameters, ζ is the spin-orbit coupling parameter and $G = 10B + 5C$, $D' = 17B + 5C$, $P = 7B + 7C$. Regarding the average

covalency parameter N , $B = N^4 B_0$, $C = N^4 C_0$, $\zeta = N^2 \zeta_0$, where ζ_0 gives free ion spin-orbit coupling parameter and B_0 and C_0 are Racah parameters for free ion [38, 40]. $\zeta_0 = 336 \text{ cm}^{-1}$, $B_0 = 960 \text{ cm}^{-1}$ and $C_0 = 3325 \text{ cm}^{-1}$ for free Mn^{2+} ion [9].

Using Racah parameters, the average covalency parameter N is found from $N = \left(\sqrt{B/B_0} + \sqrt{C/C_0} \right) / 2$. The Racah parameters ($B = 850 \text{ cm}^{-1}$, $C = 2970 \text{ cm}^{-1}$) are obtained from optical study of Mn^{2+} ion in zinc cesium sulphate hexahydrate where ligands are oxygens [41], as no optical absorption study of Mn^{2+} doped MRS is reported in literature. $[\text{Mn}(\text{H}_2\text{O})_6]^{2+}$ complexes are formed when the Mn^{2+} ion occupies the divalent sites of Zn^{2+} in zinc cesium sulphate hexahydrate and the optical absorption spectra are due to $[\text{Mn}(\text{H}_2\text{O})_6]^{2+}$ [37]. The same complex is formed in Mn^{2+} doped MRS and therefore the optical absorption spectra will be similar to Mn^{2+} in zinc cesium sulphate hexahydrate. Yoem et al. for SPM analysis of Mn^{2+} in BiVO_4 [39] have used optical spectra of Mn^{2+} : MgO due to similar ligands in the system. Hence, it appears appropriate to use Mn^{2+} optical absorption result in zinc cesium sulphate hexahydrate for Mn^{2+} doped MRS crystal.

The CF parameters are calculated using SPM [18, 39], with co-ordination factor $K_{kq}(\theta_j, \varphi_j)$ and intrinsic parameter $\bar{A}_\kappa(R_j)$, as

$$\sum_j K_{kq}(\theta_j, \varphi_j) \bar{A}_\kappa(R_j) = B_{kq}. \quad (6)$$

$\bar{A}_\kappa(R_j)$ is estimated from

$$\bar{A}_\kappa(R_0) \left(\frac{R_0}{R_j} \right)^{t_k} = \bar{A}_\kappa(R_j), \quad (7)$$

where $\bar{A}_\kappa(R_0)$ presents the intrinsic parameter, R_0 is the reference distance of the metal ion from the ligand, t_k gives power law exponent and R_j provides the ligand's distance from the d^n ion. For Mn^{2+} introduced crystals, $t_2 = 3$ and $t_4 = 7$ have been used earlier [39], the same values are taken here in our case of Mn^{2+} : MRS crystal. Since the co-ordination around Mn^{2+} ion is octahedral, \bar{A}_4 is calculated using the relation [39]

$$\bar{A}_4(R_0) = \frac{3}{4} Dq. \quad (8)$$

From optical study [41], $Dq = 790 \text{ cm}^{-1}$, which gives $\bar{A}_4(R_0) = 592.5 \text{ cm}^{-1}$. For $3d^5$ ions the ratio \bar{A}_2/\bar{A}_4 takes the value in the range 8–12 [38, 42–44]. With $\bar{A}_2 = 10\bar{A}_4$, we get $\bar{A}_2 = 5925 \text{ cm}^{-1}$.

4 Results and Discussion

Taking the ligand configuration around Mn^{2+} ion provided in Figure 1 and SPM, the CF parameters of the Mn^{2+} ion at the $\text{Mg}^{2+}(1)$ sites in MRS are calculated. Table 1 displays atoms' coordinates in single crystal of MRS with bond length R (with and without distortion) and angles θ , φ for site I. The ZFS and CF parameters as well as R_0 , reference distance is given in Table 2. Table 2 presents that $R_0 = 0.200$ nm being slightly less than the sum of radii of ions (0.223 nm) of $\text{Mn}^{2+} = 0.083$ nm and $\text{O}^{2-} = 0.140$ nm with no distortion and $\bar{A}_2/\bar{A}_4 = 8, 10, 12$ provide ZFS parameter values at octahedral substitutional site I to be quite different from the EPR experimental values [28]. Experimental parameters of ZFS $|D|$ and $|E|$ (10^{-4} cm^{-1}) for site I from EPR are 289.0, 40.0, respectively. $|E|/|D|$ is obtained as 0.138 being smaller than the standard value 0.33 [36]. $|D|$ and $|E|$ determined theoretically without distortion are larger as compared with the EPR experimental values. The value of $|E|/|D|$ is also larger than the standard value 0.33 [36]. So, local distortion is introduced into calculation. For local distortion an iterative process has been used by changing R , θ and φ to minimize the difference between calculated and experimental D and E and E/D reaching near to standard value 0.33 [36] with lattice strain being minimum at the same time. With above R_0 and local distortion, the ZFS parameter values for substitutional octahedral sites I are obtained for $\bar{A}_2/\bar{A}_4 = 8, 10, 12$ and are shown in Table 2. The ZFS parameter value $|D|$ is smaller than the experimental value (error 19.8 %) while $|E|$ is larger than the experimental one (error 23.8%) for $\bar{A}_2/\bar{A}_4 = 8$ but both $|D|$ and $|E|$ are larger for $\bar{A}_2/\bar{A}_4 = 12$ (error 22.9% for D and 142.7% for E). $|E|/|D|$ is smaller than the standard value 0.33

Table 1. Atoms' coordinates, bond length R (without and with distortion) and angles θ , φ in single crystal of MRS (site I)

Mn^{2+} position	Ligands	x	y	z	Spherical polar co-ordinates of ligands		
					R [nm]	θ [deg]	φ [deg]
Without distortion							
Site: Substitutional	O7	0.1647	0.1093	0.1618	0.20826 R_1	85.54 θ_1	85.45 φ_1
Mg(1)	O8	-0.1668	0.1101	0.0205	0.20923 R_2	89.44 θ_2	94.57 φ_2
(0.0000, 0.0000, 0.0000)	O9	-0.0041	-0.0673	0.2957	0.20307 R_3	81.62 θ_3	90.11 φ_3
	O7'	-0.1647	-0.1093	-0.1618	0.20826 R_4	94.45 θ_4	94.55 φ_4
	O8'	-0.1647	0.3907	0.6618	0.68135 R_5	84.42 θ_5	91.39 φ_5
	O9'	0.1647	0.6093	0.3382	0.79195 R_6	87.55 θ_6	88.80 φ_6
With distortion							
I	O7				0.28486	69.54	86.95
	O8				0.29923	69.44	96.57
	O9				0.31307	63.62	92.11
	O7'				0.31826	79.45	90.55
	O8'				0.82135	82.42	91.39
	O9'				0.87695	89.55	90.80

Table 2. The Mn²⁺ doped MRS crystal's CF and ZFS parameters

Site	R_0 (nm)	CF parameters (cm ⁻¹)					ZFS parameters (10 ⁻⁴ cm ⁻¹)		
		B_{20}	B_{22}	B_{40}	B_{42}	B_{44}	$ D $	$ E $	$ E / D $
Site I		Without distortion							
$\frac{\bar{A}_2}{\bar{A}_4} = 8$	0.200	-16814.9	-20763.0	5079.963	5405.05	7877.866	3195.7	1628.1	0.509
$\frac{\bar{A}_2}{\bar{A}_4} = 10$	0.200	-21018.6	-25953.8	5079.963	5405.05	7877.866	4584.4	2349.2	0.512
$\frac{\bar{A}_2}{\bar{A}_4} = 12$	0.200	-25222.4	-31144.5	5079.963	5405.05	7877.866	6268.7	3217.5	0.513
Site I		With distortion							
$\frac{\bar{A}_2}{\bar{A}_4} = 8$	0.200	-4802.2	2429.456	-6.00052	62.167	2640.437	240.6	68.1	0.283
$\frac{\bar{A}_2}{\bar{A}_4} = 10$	0.200	-6002.75	3036.82	-6.00052	62.167	2640.437	289.0	94.8	0.328
							Exp. 289.0	40.0	0.138
$\frac{\bar{A}_2}{\bar{A}_4} = 12$	0.200	-7203.31	3644.184	-6.00052	62.167	2640.437	355.1	128.7	0.362

for $\bar{A}_2/\bar{A}_4 = 8$ and larger for $\bar{A}_2/\bar{A}_4 = 12$, while $|D|$ is in good agreement with the EPR experimental value and $|E|$ is slightly larger than the experimental value for $\bar{A}_2/\bar{A}_4 = 10$ [28] but $|E|/|D|$ is very near to the standard value 0.33 [36]. Hence $\bar{A}_2/\bar{A}_4 = 10$ appears appropriate. The power law exponent parameters $t_2 = 3$ and $t_4 = 7$ with transformation S2 for standardization [36] are used to get $|E|/|D|$ ratio near to 0.33 and calculated ZFS parameters very near to experimental values obtained from EPR. Similar value of \bar{A}_2/\bar{A}_4 has been considered for Mn²⁺ doped diglycine calcium chloride tetrahydrate [45] and Fe³⁺ doped BiVO₄ [38].

The CFA computer program [46] and CF parameters B_{kq} (with distortion) are used to compute the optical spectra of Mn²⁺ doped MRS single crystals. The CF energy levels of the Mn²⁺ ion are obtained by diagonalizing the total Hamiltonian.

Table 3 presents the CF energy levels (experimental and calculated) for substitutional site I [41]. From the position and the nature of the bands observed, they have been ascribed to a Mn²⁺ ion in octahedral symmetry [41, 47]. Ligand field bands are sharp when the energy expressions for the transitions are independent of Dq , since the number of t_{2g} electrons is the same in both the excited and the ground states [47]. Consequently, the [⁴A_{1g}(G), ⁴E_g(G)] and the ⁴E_g(D) states are attributed to the sharp bands, respectively. The ⁴T_{1g}(G) and ⁴T_{2g}(G) are designated as the broad bands, respectively. These bands are broad since their transitions involve a change of configuration from $(t_{2g})^3(e_g)^2$ to $(t_{2g})^4(e_g)$. The rest of the bands are assigned to ⁴T_{2g}(G), ⁴T_{1g}(P) and ⁴T_{1g}(F) states, respectively. CFA program [46] can perform diagonalization of the full Hamiltonian

Table 3. Calculated and experimental Energy levels of single crystal of MRS doped Mn^{2+}

Transition from ${}^6\text{A}_{1g}(\text{S})$ state	Observed (cm^{-1})	Calculated (cm^{-1}) I
${}^4\text{T}_{1g}(\text{G})$	18436	23547, 23556, 23778, 23839, 24032, 24098
${}^4\text{T}_{2g}(\text{G})$	22815	24203, 24218, 24444, 24482, 24523, 24565
${}^4\text{E}_g(\text{G})$	24783	24833, 24862, 24865, 24874
${}^4\text{A}_{1g}(\text{G})$	24850	24883, 24895
${}^4\text{T}_{2g}(\text{D})$	28003	26767, 27150, 27216, 28762, 28768, 29194
${}^4\text{E}_g(\text{D})$	29870	29232, 29735, 29814, 30242
${}^4\text{T}_{1g}(\text{P})$	32435	31211, 31243, 35163, 35254, 35372, 35462
${}^4\text{A}_{2g}(\text{F})$		36454, 36796
${}^4\text{T}_{1g}(\text{F})$	41460	40982, 41109, 41226, 41275, 41365, 41480

within the $3d^N$ basis of states in the intermediate crystal field coupling scheme providing not only the CF energy levels but also the state vectors. The crystal field Hamiltonian, Trees correction (α), the Coulomb interaction (in terms of the Racah parameters B and C), the spin-orbit interaction (ζ), the spin-spin interaction (M_0), and the spin-other orbit interaction (two parameters: M_{00} , M_{22}) are all included in the Hamiltonian used in the CFA program. The free-ion parameters used in the CFA computations have the following values: $\zeta_0 = 336$, $B = 850$ and $C = 2970$, $\alpha = 76 \text{ cm}^{-1}$, $M_{00} = 0.2917$, $M_{22} = 0.0229$, $M_0 = 0.2917$ and $M_2 = 0.0229$. Though the whole Mn^{2+} spectra consist of 120 degenerate states, we show only a few energy levels based on intensity [48]. The transitions associated with ${}^4\text{E}_g(\text{G})$, ${}^4\text{A}_{1g}(\text{G})$, ${}^4\text{E}_g(\text{D})$, ${}^4\text{T}_{2g}(\text{D})$, ${}^4\text{A}_{2g}(\text{F})$ and ${}^4\text{T}_{1g}(\text{F})$ are well predicted while the transitions associated with ${}^4\text{T}_{1g}(\text{G})$, ${}^4\text{T}_{2g}(\text{G})$, ${}^4\text{T}_{1g}(\text{P})$ and ${}^4\text{T}_{1g}(\text{F})$ show larger deviation. The reasons for larger deviations may be vibronic coupling, electron correlation effects or limitations of the CF model [37].

Table 3 presents that the experimental and calculated energy levels correspond reasonably well. Thus, the theoretical study verifies the EPR experimental result [28, 41] that Mn^{2+} ions enter the MRS crystal at substitutional $\text{Mg}^{2+}(\text{I})$ octahedral site. ZFS parameter computations for Mn^{2+} ions at suitable molecular nano magnet sites may make application of the obtained model parameters.

5 Conclusions

To find the splitting parameters of crystal-field and zero field, the superposition model and perturbation theory are applied for Mn^{2+} ions introduced MRS single crystals. The computed ZFS parameters for $\bar{A}_2/\bar{A}_4 = 10$ are in good agreement with the results of the EPR experiment. The values from the experiment and the computed CF energy levels agree pretty well. Consequently, the theoretic-

cal study verifies the conclusion of the EPR experiment that Mn^{2+} ions replace Mg^{2+} (1) sites in MRS crystal. The parameters of ZFS for Mn^{2+} ions in molecular nanomagnets at similar locations may be determined using the obtained model parameters in this study. The above modeling procedure may be helpful in finding many crystals with different applications in science and industry.

Acknowledgement

The authors thank Prof. C. Rudowicz of the Faculty of Chemistry at Adam Mickiewicz University in Poznan, Poland, for the CFA program, and the Head of the Physics Department at Allahabad University in Allahabad for providing departmental facilities.

References

- [1] P.S. Rao, S. Subramanian (1985) Single crystal E.P.R. studies of some first-row transition ions in hexaimidazole zinc(II)dichloride tetrahydrate, IV. $\text{Mn}(\text{II})$: A case of twinning. *Mol. Phys.* **54** 429-438.
- [2] Y.N. Naidu, J.L. Rao, S.V.J. Lakshman (1992) Electron paramagnetic resonance and optical absorption spectra of Mn^{2+} in magnesium malate pentahydrate (MMPH) single crystals. *Solid State Commun.* **81** 437-442.
- [3] P.S. Rao (1993) Single crystal EPR study of $\text{Mn}(\text{II})$ -doped magnesium potassium Tutton's salt. *Spectrochim. Acta A* **49** 897-901.
- [4] S.K. Misra (1994) Estimation of the Mn^{2+} zero-field splitting parameter from a polycrystalline EPR spectrum. *Physica B* **203** 193-200.
- [5] J.A. Weil, J.R. Bolton (2007) *Electron Paramagnetic Resonance: Elementary Theory and Practical Applications* 2nd ed. Wiley, New York.
- [6] D. Halder, Y. Jana, D. Piwowarska, P. Gnutek, C. Rudowicz (2024) Tailoring single-ion magnet properties of coordination polymer $\text{C}_{11}\text{H}_{18}\text{DyN}_3\text{O}_9$ (Dy-CP) using the radial effective charge model (RECM) and superposition model (SPM). *Phys. Chem. Chem. Phys.* **26** 19947-19959.
- [7] S.P. Rathee, S.S. Hooda (2025) EPR and superposition-model analysis of zero-field splitting parameters for Mn^{2+} doped in $\text{ZnNbOF}_5 \cdot 6\text{H}_2\text{O}$ and $\text{CoNbOF}_5 \cdot 6\text{H}_2\text{O}$ single crystals. *Indian J. Phys.* **99** 145-148.
- [8] V.K. Jain, G. Lehmann (1990) Electron Paramagnetic Resonance of Mn^{2+} in Orthorhombic and Higher Symmetry Crystals. *Phys. Status Solidi b* **159** 495-544.
- [9] D.J. Newman (1982) Superposition model analysis of spin Hamiltonian parameters. *J. Phys. C: Solid State Phys.* **15** 6627-6630.
- [10] C. Rudowicz, P. Gnutek, M. Açıkgöz (2019) Superposition model in electron magnetic resonance spectroscopy – a primer for experimentalists with illustrative applications and literature database. *Appl. Spectrosc. Rev.* **54** 673-718.
- [11] A. Abragam, B. Bleaney (1986) *Electron Paramagnetic Resonance of Transition Ion*. Dover, New York.
- [12] J.R. Pilbrow (1990) *Transition-Ion Electron Paramagnetic Resonance*. Clarendon Press, Oxford.

- [13] B.G. Wybourne (1965) *Spectroscopic Properties of Rare Earth*. Wiley, New York.
- [14] J. Mulak, Z. Gajek (2000) *The Effective Crystal Field Potential*. Elsevier, Amsterdam.
- [15] R. Boča (2004) Zero-field splitting in metal complexes. *Coord. Chem. Rev.* **248** 757-815.
- [16] Y.Y. Yeung (2013) in: *Optical Properties of 3d-Ions in Crystals: Spectroscopy and Crystal Field Analysis*, eds. M.G. Brik, N.M. Avram. Heidelberg: Springer, Chapter 3, pp. 95-121.
- [17] A.K. Yadav, U.M. Tripathi, R. Kripal (2022) Theoretical Calculation of Zero-Field Splitting Parameters for Mn^{2+} in Potassium Hydrogen Sulphate. *Appl. Magn. Reson.* **53** 941-947.
- [18] D.J. Newman, B. Ng (1989) The superposition model of crystal fields. *Rep. Prog. Phys.* **52** 699-763.
- [19] D.J. Newman, E. Siegel (1976) Superposition model analysis of Fe^{3+} and Mn^{2+} spin-Hamiltonian parameters. *J. Phys. C: Solid State Phys.* **9** 4285-4292.
- [20] Y.Y. Yeung (1988) Local distortion and zero-field splittings of $3d^5$ ions in oxide crystals. *J. Phys. C: Solid State Phys.* **21** 2453-2462.
- [21] F. Bosi, G. Belardi, P. Ballirano (2009) Structural features in Tutton's salts $K_2[M^{2+}(H_2O)_6](SO_4)_2$, with $M^{2+} = Mg, Fe, Co, Ni, Cu,$ and Zn . *Am. Mineral.* **94** 74-82.
- [22] M. Wildner, D. Marinova, D. Stoilova (2016) Vibrational spectra of $Cs_2Cu(SO_4)_2 \cdot 6H_2O$ and $Cs_2Cu(SeO_4)_2 \cdot nH_2O$ ($n=4, 6$) with a crystal structure determination of the Tutton salt $Cs_2Cu(SeO_4)_2 \cdot 6H_2O$. *J. Mol. Struct.* **1106** 440-51.
- [23] H.T. Montgomery, E.C. Lingafelter (1964) The crystal structure of Tutton's salts. II. Magnesium ammonium sulfate hexahydrate and nickel ammonium sulfate hexahydrate. *Acta Cryst.* **17** 1478-9.
- [24] M. de Oliveira, S. Ghosh, T.S. Pacheco, G.J. Perpétuo, C.J. Franco (2017) Growth and structural analysis of ammonium nickel cobalt sulfate hexahydrate crystals. *Mater. Res. Express* **4** 105036.
- [25] A. Abu El-Fadl, A.M. Nashaat (2017) Growth, structural, and spectral characterizations of potassium and ammonium zinc sulfate hydrate single crystals. *Appl. Phys. A* **123** 339(11 pages).
- [26] K.H. Büchel, H.H. Moretto, P. Woditsch (2008) *Industrial Inorganic Chemistry*. Weinheim: Wiley-VCH.
- [27] D.L. Perry (2016) *Handbook of Inorganic Compounds*. CRC Press, Boca Raton, Florida, USA
- [28] V.K. Jain (1977) EPR of Mn^{2+} in Tutton Salts. *Z. Naturforsch.* **32** 1364-1367.
- [29] W.L. Yu, M.G. Zhao (1988) Spin-Hamiltonian parameters of 6S state ions. *Phys. Rev. B* **37** 9254-9267.
- [30] G. Aromí, E.K. Brechin (2006) Synthesis of 3d metallic single-molecule magnets. *Struct. Bonding* **122** 1-67.
- [31] C. Coulon, H. Misayaka, R. Clérac (2006) Single-Chain Magnets: Theoretical Approach and Experimental Systems. *Struct. Bonding* **122** 163-206.
- [32] M. Murrie, (2010) Cobalt(ii) single-molecule magnets. *Chem. Soc. Rev.* **39** 1986-1995.

- [33] C. van Wüllen (2013) Magnetic anisotropy through cooperativity in multinuclear transition metal complexes: theoretical investigation of an anisotropic exchange mechanism. *Mol. Phys.* **111** 2392-2397.
- [34] H. Euler, B. Barbier, S. Klumpp, A. Kirfel (2000) Crystal structure of Tutton's salts, $\text{Rb}_2[\text{M}^{II}(\text{H}_2\text{O})_6](\text{SO}_4)_2$, $\text{M}^{II} = \text{Mg, Mn, Fe, Co, Ni, Zn}$. *Z. Kristallogr. NCS* **215** 473-476.
- [35] C.J. Radnell, J.R. Pilbrow, S. Subramanian, M.T. Rogers (1975) Electron paramagnetic resonance of Fe^{3+} ions in $(\text{NH}_4)_2\text{SbF}_5$. *J. Chem. Phys.* **62** 4948-4952.
- [36] C. Rudowicz, R. Bramley (1985) On standardization of the spin Hamiltonian and the ligand field Hamiltonian for orthorhombic symmetry. *J. Chem. Phys.* **83** 5192-5197.
- [37] B.N. Figgis, M.A. Hitchman (2000) *Ligand Field Theory and its Applications*. Wiley, New York.
- [38] T.H. Yeom, S.H. Choh, M.L. Du, M.S. Jang (1996) EPR study of Fe^{3+} impurities in crystalline BiVO_4 . *Phys. Rev. B* **53** 3415-3421.
- [39] T.H. Yeom, S.H. Choh, M.L. Du (1993) A theoretical investigation of the zero-field splitting parameters for an Mn^{2+} centre in a BiVO_4 single crystal. *J. Phys.: Condens. Matter* **5** 2017-2024.
- [40] C. K. Jorgensen (1971) *Modern Aspects of Ligand Field Theory*. North-Holland, Amsterdam.
- [41] K. Purandar, J.L. Rao, S.V.J. Lakshman (1984) Optical Absorption Spectrum of Mn^{2+} in Zinc Cesium Sulphate Hexahydrate. *Acta Phys. Slov.* **34** 195-207.
- [42] D.J. Newman, B. Ng (2000) *Crystal Field Handbook*. Cambridge University Press, Cambridge.
- [43] A. Edgar (1976) Electron paramagnetic resonance studies of divalent cobalt ions in some chloride salts. *J. Phys. C: Solid State Phys.* **9** 4303-4314.
- [44] R. Kripal, M.G. Misra, A.K. Yadav, P. Gnutek, M. Açıköz, C. Rudowicz (2023) Theoretical Analysis of Crystal field Parameters and Zero field Splitting Parameters for Mn^{2+} ions in Tetramethylammonium Tetrachlorozincate. *Polyhedron* **235** 116341.
- [45] S. Pandey, R. Kripal (2014) A Theoretical Analysis of Zero Field Splitting Parameters of Mn^{2+} Doped Diglycine Calcium Chloride Tetrahydrate. *Chin. J. Phys.* **52** 262-271.
- [46] Y. Y. Yeung, C. Rudowicz (1993) Crystal Field Energy Levels and State Vectors for the $3d^N$ Ions at Orthorhombic or Higher Symmetry Sites. *J. Comput. Phys.* **109** 150-152.
- [47] Y. Tanabe, S. Sugano (1954) On the Absorption Spectra of Complex Ions. I. *J. Phys. Soc. Jpn.* **9** 753-766.
- [48] Y.Y. Yeung, C. Rudowicz, Y.M. Chang, J. Qin (1994) Model calculation of the spectroscopic properties for Cr^{3+} Kyanite. *J. Lumin.* **60&61** 108-111.